Chaotic behavior, collective modes, and self-trapping in the dynamics of three coupled Bose-Einstein condensates

Roberto Franzosi[1] and Vittorio Penna[2]
[1]*Dipartimento di Fisica dell'Università di Pisa and INFN, Sezione di Pisa, Via Buonarroti 2, I-56127 Pisa, Italy*
[2]*Dipartimento di Fisica and UdR INFM, Torino Politecnico, Corso Duca degli Abruzzi 24, I-10129 Torino, Italy*
(Received 15 November 2001; revised manuscript received 3 October 2002; published 30 April 2003)

The dynamics of the three coupled bosonic wells (trimer) containing N bosons is investigated within a standard (mean-field) semiclassical picture based on the coherent-state method. Various periodic solutions (configured as π-like, dimerlike, and vortex states) representing collective modes are obtained analytically when the fixed points of trimer dynamics are identified on the $N=$const submanifold in the phase space. Hyperbolic, maximum and minimum points are recognized in the fixed-point set by studying the Hessian signature of the trimer Hamiltonian. The system dynamics in the neighborhood of periodic orbits (associated with fixed points) is studied via numeric integration of trimer motion equations, thus revealing a diffused chaotic behavior (not excluding the presence of regular orbits), macroscopic effects of population inversion, and self-trapping. In particular, the behavior of orbits with initial conditions close to the dimerlike periodic orbits shows how the self-trapping effect of dimerlike integrable subregimes is destroyed by the presence of chaos.

DOI: 10.1103/PhysRevE.67.046227 PACS number(s): 05.45.−a, 03.75.Kk, 03.65.Sq

I. INTRODUCTION

Remarkable progress in experimental design has been made since the first direct observation of Bose-Einstein condensation in dilute atomic gas [1]. One of the most promising developments concerns the construction of experimental devices in which condensates, achieved within complex geometries, interact with each other giving rise to quantum effects that are observable at the macroscopic level [2–4]. In this respect, one should recall, for example, the (superfluid) boson Josephson-junction arrays obtained by means of optical lattices that trap weak interacting Bose-Einstein condensates (BECs) in periodic arrays of potential wells [5]. In parallel with the experimental work, increasing attention has been devoted theoretically to studying the dynamical behavior of low-energy states [6] in arrays of Bose-Einstein condensates where the number of lattice sites (namely, the potential wells occupied by the condensate) is very large [7,8].

Opposite situations, corresponding to ''lattices'' formed by two or three interacting wells, have been investigated as well in various recent papers (see Refs. [9–14]). In particular, the two-well system (dimer) has been analyzed thoroughly from both the semiclassical (mean-field) and the purely quantum viewpoint in Refs. [10,14], respectively. Such investigations have revealed how the nontrivial structure of dimer phase space causes many significant phenomena such as the symmetry-breaking effect (issuing oscillation modes that are isoenergetic but nonequivalent), the onset of π-phase oscillations, the *self-trapping* of boson populations, and, quantum mechanically, the occurrence of (parameter-dependent, nondegenerate) doublets in the energy spectrum entailing periodic self-trapping.

The addition of a third well to the dimer system suggests that an even richer dynamics should be observed: The resulting system, in fact, is no longer integrable. This fact and the forthcoming realization of such system (due to the great experimental progress in the confinement techniques) indeed prompt the theoretic study of the three-well system (*trimer*) that is the central topic of this paper. In particular, the study of trimer offers the possibility to investigate regimes of special interest, where the competition of the (purely quantum) integrable evolution with the (classical) chaotic behavior takes place, in the limit of large number of atoms.

The connection between the quantum and the semiclassical picture of many interacting bosonic wells has been illustrated in Ref. [10] and, in view of the closed link between an array of interacting BECs and the Bose-Hubbard (BH) model [10,15], in Ref. [16] within the BH model theory. We wish to observe that the semiclassical approach (corresponding to describing condensates within the Bogoliubov approximation) is appropriate for interacting wells with macroscopic boson populations. However, the systems recently obtained (where mesoscopic numbers of bosons per wells [4] have been achieved in condensates distributed among many wells) might be best modeled by using the space-mode approximation [9,17] stemmed from the second-quantized boson-field theory.

Compared with the dimer nonlinear behavior, indeed the system of three interacting bosonic wells exhibits an unexpectedly rich phenomenology and provides an interesting research topic, both theoretically and experimentally. In fact, despite the simplicity of the model, the trimer dynamics is affected by a strong inner instability leading to the chaos onset. This feature originates from the combination of the model nonlinear character with the nonintegrable nature that distinguishes trimer dynamics within extended regions of its phase space. In respect of this, the solutions of the trimer dynamical equations [displaying nonlinear periodic oscillations (dimerlike orbits) with possible self-trapping effect] recognized in Refs. [11,13] must be viewed as special subregimes in which dynamics is integrable. Concerning the instability of trimer dynamics, we wish to recall that the presence of homoclinic chaos has been revealed for the asymmetric trimer in Ref. [18]. Also, the trap anisotropy of a condensate, which induces space separation, has been seen as

an instability source in Ref. [19]. An alternative study of such instability is in progress, based on the geometrical approach recently proposed in Refs. [20,21]. Such approach consists in tackling the Hamiltonian chaos relying on the fact that the geometry involved by the trimer Hamiltonian is that of the Finsler spaces [22]. At the quantum level, the survival of trimer breather configurations has been investigated in Ref. [23], while trimerlike systems (or systems involving more complex bosonic lattices) have been studied recently [24,25] within the quantum-computation physics.

In the present paper, we perform a systematic analysis of the trimer dynamics directed to ascertain that the abscence of integrability generates chaos and that this dominates the interactions of three BECs modeled in a standard semiclassical picture. A rich scenario of dynamical behaviors emerges from our analysis, which confirms the extremely structured character of trimer dynamics and represents the natural prosecution of the work of Ref. [13], in which we focused our attention on the special dimerlike (integrable) regime of trimer and on the self-trapping effect.

Moreover, our analysis furnishes a complete scenario of the trimer dynamical regimes and of their dependence on the external parameters occurring in the Hamiltonian (notice that the control on the parameters' dependence is expected to be operationally useful in relation to experiments). It appears as well to be topical in relation to the study of the dynamics of solitons [8] and of vortices [26] on one-dimensional chains of BECs as well as of experimental architectures obtained recently [4]. The observation of such chain excitations, in fact, must take into account the possible destructive action of inner instabilities whose influence is clearly manifested in the trimer chain. We emphasize the fact that the trimer chain is the simplest possible situation in which interacting BECs turns out to be governed by nonintegrable equations. The dimer dynamics, in fact, is completely integrable.

The paper layout is the following. In Sec. II, we review the derivation of the space-mode Hamiltonian for three coupled wells from the quantum field theory of bosonic fluids in the dilute-gas approximation, and present the semiclassical picture that describes coupled boson wells with macroscopic populations. In Sec. III, we identify the set of fixed points of the trimer Hamiltonian equations and show how such points are associated to periodic solutions (representing collective modes) owing to the dynamically conserved total boson number N. Section IV is devoted to study the second variation (with $N=\text{const}$) of the energy function for such extremal configurations in order to make explicit their nature. In Sec. V, we perform a dimensional reduction of trimer dynamics by defining a new set of canonical variables whereby the constant of motion N is incorporated in the dynamical equations. This paves the way to the implementation of the Poincaré sections' method. The chaos onset in the trimer dynamics is investigated in Sec. VI. First, in a qualitative way, by constructing the Poincaré sections for trajectories whose initial conditions are chosen in proximity of the fixed-point configurations identified in Sec. III. Then, quantitatively, by measuring the maximum Lyapunov exponent of such trajectories. Section VII contains concluding remarks and comments on future work.

II. TRIMER DYNAMICS

The model for a chain (or more complex structures) of M interacting bosonic wells can be derived from the quantum field theory for boson fluids (with a nonlocal ψ^4 term) by implementing the M-(space)mode approximation [15]. If the boson fluid is a diluite gas of N interacting bosons trapped in an external potential V_e then its dynamics is generated by the local boson-field Hamiltonian [17,28,27]

$$\hat{H}=\int d\mathbf{r}\,\hat{\psi}^{\dagger}(\mathbf{r})\left[V_e-\frac{\hbar^2\nabla^2}{2m}+\frac{U_0}{2}\hat{\psi}^{\dagger}(\mathbf{r})\hat{\psi}(\mathbf{r})\right]\hat{\psi}(\mathbf{r}),$$

where m is the boson mass, $U_0=4\pi\hbar^2 a/m$ takes into account the two-body interaction strength, and a is the s-wave scattering length. The field $\psi(\mathbf{r})$ $[\hat{\psi}^{+}(\mathbf{r})]$ is the Heisenberg field operator that destructs (creates) bosons at position $\mathbf{r}$. The nonlinear term has been written in the usual normal ordered form. In order to work out the trimer Hamiltonian, we state some assumptions: First, V_e is a three-well symmetric-shaped potential. Second, the lowest-energy level of each well (within the approximation of V_e in terms of a single-well parabolic potential) must be well separated from the higher-energy levels [17]. Third, the binary particle interactions is not strong enough to significatively change the latter assumptions.

Some further approximations are necessary to make explicit the ground-state structure in $\hat{H}$. Let $\mathbf{r}_i$ $(i=1,2,3)$ be the locations of the minima of V_e and let $V_j=V(\mathbf{r}-\mathbf{r}_j)$ be the parabolic approximation to the potential in the jth minimum, so that $V_e(\mathbf{r})\simeq V(\mathbf{r}-\mathbf{r}_j)$ when $\mathbf{r}\simeq\mathbf{r}_j$. Also, let us introduce the eigenstates u_j that represent the normalized single-boson ground states with energy E_0 of the local parabolic potential V_j. These states are only approximatively orthogonal because of $\int d^3\mathbf{r}\overline{u_j}u_k=\delta_{jk}+R_{jk}$ but the residue R_{jk} is a quantity exponentially suppressed depending on the overlap between u_j and u_k. The analysis is restricted to those potentials for which $R_{jk}\ll 1$ thus making negligible such contributions.

The picture of the system thus resulting suggests that the boson field operator can be expanded as $\hat{\psi}(\mathbf{r},t)=\Sigma_i\overline{u_i}(\mathbf{r})\hat{a}_i(t)$, where $\hat{a}_i(t)$ $[\hat{a}_i^{\dagger}(t)]$ is the annihilation (creation) boson operator (associated to the space-mode state u_i) that satisfy the commutation relation $[\hat{a}_i(t),\hat{a}_k^{\dagger}(t)]=\delta_{ik}$. By substituting this expression in the many-body hamiltonian one can obtain, to the lowest order in the overlap between the single-well modes, the quantum trimer Hamiltonian [10,11]

$$H_3=\sum_i\,[U(n_i-1)-v]n_i-\frac{T}{2}\sum_{\langle i,j\rangle}(a_i^{\dagger}a_j+a_j^{\dagger}a_i),$$

where the site index $i,j=1,2,3$, $v=-E_0$, and the operators $n_i\doteq a_i^{\dagger}a_i$ count the number of bosons at site i. Also, in H_3

$$T=2\int d^3\mathbf{r}\overline{u_j}[V_j-V_e]u_{j\pm 1},\quad U=\frac{U_0}{2}\int d^3\mathbf{r}|u_j|^4,$$

represent the (interwell) hopping amplitude and the strength of the Coulomb on-site repulsion, respectively [9,17].

The quantum dynamics involved by Hamiltonian H_3 can be cast in a classical form by representing the system quantum state through a trial state $|Z\rangle$ written in terms of Glauber's states $|z_i\rangle$ (defined by $a_i|z_i\rangle = z_i|z_i\rangle$). By implementing the time-dependent variational principle (TDVP) and the procedure discussed in Refs. [16,29] on $|Z\rangle = \Pi_i|z_i\rangle$, one obtains the effective Hamiltonian [10]

$$\mathcal{H}_3(Z,Z^*) := \langle Z|H_3|Z\rangle \equiv \sum_{j=1}^{3}\left[U|z_j|^4 - v|z_j|^2 - \frac{T}{2}(z_j^* z_{j+1} + \text{c.c.})\right] \tag{1}$$

($j=1\equiv 4$ on the trimer chain) with the equations

$$\begin{aligned} i\hbar\dot{z}_1 &= (2U|z_1|^2 - v)z_1 - \frac{T}{2}(z_2+z_3),\\ i\hbar\dot{z}_2 &= (2U|z_2|^2 - v)z_2 - \frac{T}{2}(z_3+z_1),\\ i\hbar\dot{z}_3 &= (2U|z_3|^2 - v)z_3 - \frac{T}{2}(z_1+z_2). \end{aligned} \tag{2}$$

Such equations for z_j (notice that $z_j \equiv \langle Z|a_j|Z\rangle$ and $z_j^* = \langle Z|a_j^\dagger|Z\rangle$) can be calculated from $\mathcal{H}_3$ via the Poisson brackets $\{z_k^*, z_j\} = i\delta_{k,j}/\hbar$ furnished by the TDVP method. Those for z_j^* are easily obtained by complex conjugation. Various aspects concerning the special dimerlike subregime of Eqs. (2), in which trimer dynamics is integrable, have been studied in Refs. [11,13].

III. FIXED POINTS AND PERIODIC ORBITS

The distinctive features that characterize the dynamics of a given Hamiltonian system can be recognized by exploring the structure of its phase space. The first step to do this [33] is to locate the fixed points and to find their dependence on the model parameters U, T. The fixed points are derived in the present section based on Eqs. (2), whereas the nature of such points is studied in the following section.

The fixed-point equations for the trimer are obtained by setting $\dot{z}_j \equiv 0$ in Eqs. (2). Since the trimer dynamics is constrained by the constant of motion $N = |z_1|^2 + |z_2|^2 + |z_3|^2$, one must incorporate explicitly the restriction to the phase-space submanifold defined by $N=\text{const}$ through a Lagrange multiplier χ. This just requires that one considers the variations of $\mathcal{H}_3 - \chi N$ in place of that of $\mathcal{H}_3$. The resulting equations are

$$0 = \left(2U|z_j|^2 - \mu + \frac{T}{2}\right)z_j - \frac{T}{2}Z, \tag{3}$$

where $j=1,2,3$, and $Z := z_1+z_2+z_3$, $\mu := \chi + v$ have been introduced. Therefore, any fixed point, namely, any vector $(z_i) \equiv (\eta_1, \eta_2, \eta_3)$ that satisfies Eqs. (3), provides, at the same time, a dynamically active solution of Eqs. (2) represented by $z_j(t) = \eta_j \exp[i\chi t/\hbar]$. Despite its time dependence, such a *periodic orbit* represents a (one-dimensional) extremal configuration of $\mathcal{H}_3$ on the hypersurface $N=\text{const}$. The solutions of Eqs. (3) can be grouped in various classes the first of which is represented by the case

$$Z = \sum_j z_j = 0.$$

The remaining cases are obtained from Eqs. (A3) and (A4), where z_i can be replaced with the real quantities x_i (see Appendix A). Such cases are given by

$$x_1 = x_2 = x_3 \neq 0,$$

$$x_1 = -x_2 \neq x_3 = 0,$$

$$x_1 = x_2 \neq x_3 \neq 0.$$

Such configurations are discussed below [30].

A. Ground-state configurations

When $x_1 = x_2 = x_3$, Eqs. (A3) and (A4) are satisfied. Based on Eq. (A2) combined with the conserved quantity N, one finds that $x_j = \pm\sqrt{N/3}$ which provides

$$z_i = \sqrt{N/3}\exp(i\Phi) \quad (i=1,2,3), \tag{4}$$

and $3\mu = 2UN - 3T$. The energy of such configurations (they are shown to represent the ground state in Sec. III) is given by

$$E_{gs} = \frac{1}{3}UN^2 - TN. \tag{5}$$

The ground-state phase Φ is arbitrary since it represents a symmetry of the model. Also, the fact that $z_j = |z_j|\exp(i\phi_j)$ have the same phase $\phi_j \equiv \Phi$ reproduces the symmetry breaking phenomenon that distinguishes the minimum energy state and, particularly, the vanishing of the phase difference (between closed points) in superfluid media. Such two features, which are known to characterize the superfluid ground state of BH lattice model, naturally extend to the trimer model of condensates in our semiclassical picture. As regards Eqs. (2), they are solved by $z_j(t) = \sqrt{N/3}\exp[i(\Phi + \chi t/\hbar)]$, with $\chi = \mu - v$, that describes the ground-state collective mode.

B. Vortexlike configurations

The situation in which $Z=0$ leads to a special configuration. In this case Eqs. (3) reduce to $0 = (2U|z_j|^2 - \mu + T/2)z_j$ implying, in turn, that

$$|z_j|^2 = \frac{2\mu - T}{4U}, \quad \forall\, j, \quad \mu = \frac{4NU + 3T}{6},$$

where the value of μ is derived from $\Sigma_i|z_i|^2 = N$. As a consequence of the independence of $|z_j|$ on the site index, the

condition $Z=0$ is realized only if the phases of $z_j=|z_j|\exp(i\theta_j)$ are such that $\theta_j(k)=2\pi jk/3+\Phi_0$, where $k=1,2$, and Φ_0 is an arbitrary phase. This configuration represents a particular case of the vortex state discussed for the Bose-Hubbard model on a M-well chain lattice ($M>2$) in Refs. [26] and [10]. The energy associated with the vortex states,

$$z_j(k)=\sqrt{N/3}\exp[i\theta_j(k)], \tag{6}$$

is given by

$$E_v=\frac{UN^2}{3}-TN\cos\left(\frac{2\pi}{3}k\right)=\frac{UN^2}{3}+\frac{TN}{2}, \tag{7}$$

while dynamics issued from Eq. (2) is described by the solution $z_j(t)=z_j(k)\exp[it(\mu-v)/\hbar]$.

C. Configurations with a single depleted well

These configurations are characterized by the presence of a single depleted well (SDW). Without losing generality, one can choose the second well, so that one has $x_1,x_3\neq 0$ and $x_2=0$. This case can be faced based on Eqs. (A1): to satisfy $E_2(\mathbf{x})=0$ one must impose $x_3=-x_1$, which entails, in turn, that the equation $E_1(\mathbf{x})=0$ is equivalent to the equation $E_3(\mathbf{x})=0$. The latter, together with the constraint $N=x_1^2+x_3^2$, implies that $x_1=\pm\sqrt{N/2}=-x_3$, $x_2=0$, which provides the fixed points

$$z_1=\sqrt{N/2}e^{i\Phi},\quad z_2=0,\quad z_3=\sqrt{N/2}e^{i(\Phi+\pi)}, \tag{8}$$

with $\mu\equiv 2Ux_1^2+T/2$. Their energy is

$$E_{\mathrm{DW}}=\frac{1}{2}UN^2+\frac{1}{2}TN. \tag{9}$$

Permutations of site indices j of z_j furnish other five fixed points of the same type. In view of state (8), it is worth noting that SDW configurations have the same structure of the π *states* occurring in the dimer dynamics [10], where the phases of each well keep a constant phase difference π in the course of time evolution. Solutions $z_i(t)=z_i(0)\exp[it(\mu-v)/\hbar]$—with $z_i(0)$ given by Eqs. (8)—exhibit this property.

D. Dimerlike configurations

For such states the variables x_j (recall that x_j^2 is the boson number of the jth well) satisfy the condition $x_i=x_j\neq x_k$. Three cases are thus obtained through index permutation. In general, since three fixed points turn out to be associated with each dimerlike configuration (namely, to each choice $x_i=x_j\neq x_k$), nine fixed points are finally found in the dimerlike class.

To deal with an explicit case, we shall consider the fixed points of the case $x_1=x_2\neq x_3$. Owing to its complexity, their derivation is described in Appendix B. Here, we discuss the results obtained. Fixed points depend on the parameter $\tau:=T/NU$ and are representable as points $(x_1,x_2,x_3)\in\mathbb{R}^3$ on a sphere due to the constraint $N=\Sigma_i x_i^2$. Their expressions read

$$\begin{aligned}
A_1&:=(a_1,a_1,-(a_1/|a_1|)\sqrt{N-2a_1^2}),\\
A_2&:=(a_2,a_2,-(a_2/|a_2|)\sqrt{N-2a_2^2}),\\
A_3&:=(a_3,a_3,-(a_3/|a_3|)\sqrt{N-2a_3^2}),
\end{aligned} \tag{10}$$

where

$$a_3=\pm\left[\frac{Np^2}{1+2p^2}\right]^{1/2},\quad a_\nu=\pm\left[\frac{N}{2+q_\nu^2}\right]^{1/2}, \tag{11}$$

and $\nu=1,2$. Parameters q_ν and p are defined as implict functions of parameter τ through systems (B3) and (B4), respectively. In particular, the cubic equation

$$\tau(2+q^2)(2+q)+4q(1+q)=0, \tag{12}$$

derived from Eq. (B3), with $q\in[-1,0]$ furnishes the τ functions $q_1(\tau)$, $q_2(\tau)$ corresponding to the real roots of Eq. (12). Notice that $-1\leqslant q_1(\tau)<q_2(\tau)\leqslant 0$ for $\tau<\tau^*$, whereas, for $\tau>\tau^*$, there are no solutions. The value τ^*, where $q_1(\tau^*)=q_2(\tau^*)$ (and $A_1\equiv A_2$), is calculated in Appendix B. Instead, system (B4), with $p\in[-1/2,0]$, always exhibits a single solution $p(\tau)$ that is carried out from the equation

$$\tau(1+2p^2)(1+2p)+4p(1+p)=0. \tag{13}$$

The dependence on physical parameters T, U, N of $A_1(q_1)$, $A_2(q_2)$, $A_3(p)$ by means of parameter τ is thus established.

Points A_i found in this way generate, by varying τ, three curves on the sphere with $N=\mathrm{const}$ [in view of the sign $\pm$ in Eqs. (11) they actually are six]. These become 18 when considering the fixed points generated by index permutations. This process is described in Appendix B, where the actual number of dimerlike fixed points is shown to reduce to 12. Such curves [parametrized by τ via $p(\tau)$ and $q_\nu(\tau)$] can be proven to never intersect with one another except for the special case $\tau=\tau^*$, where $A_1\equiv A_2$. This *coalescence* effect is discussed below.

If the values of q_ν and p for some given $\tau\leqslant\tau^*$ are carried out explicitly, the energy for A_i,

$$E_d=U[N^2+6a_i^4-4Na_i^2]-T[a_i^2-2a_i\sqrt{N-2a_i^2}] \tag{14}$$

$(i=1,2,3)$, is obtained via formulas (11).

We conclude illustrating the physical situations that correspond to configurations A_1, A_2, and A_3 when τ changes. Also, we compare them to the *pure-dimer* scenario [10]. Let us start with $\tau\to 0$. One has $q_1=-1$ and $q_2=p=0$ that entail

$$\begin{aligned}
A_1(-1)&:=\pm(\sqrt{N/3},\sqrt{N/3},-\sqrt{N/3}),\\
A_2(0)&:=(\sqrt{N/2},\sqrt{N/2},0),
\end{aligned} \tag{15}$$

$$A_3(0) := (0,0,\sqrt{N}),$$

respectively. By increasing τ, $A_1(q_1)$ and $A_2(q_2)$ get closer and closer ($A_1 = A_2$ for $\tau \to \tau_*$). When $\tau > \tau_*$ only the fixed point $A_3(p)$ survives. In particular, $\tau \to \infty$ implies $p = -1/2$, so that [from the third equation of Eqs. (10)] one obtains

$$A_3\left(-\frac{1}{2}\right) = \pm(\sqrt{N/6}, \sqrt{N/6}, -\sqrt{2N/3}). \tag{16}$$

Since $A_3(p)$ [as well as $B_3(p)$, $C_3(p)$, obtained via index permutation (see Appendix B)] is shown to be a maximum in Sec. IV, indeed $A_3(p)$ appears to be comparable with the τ-dependent maximum of the (pure) dimer model [10], where a unique well ends up being filled when $\tau \to 0$. Instead, when τ is increased, no merging of $A_3(p)$ with other maxima [e.g., $B_3(p)$, $C_3(p)$] happens as that observed in the (pure) dimer model. In this model, in fact, a (macroscopic) coalescence effect takes place (see, Ref. [10]) since two maxima merge in a unique one when $\tau > 1$ [the opposite effect (bifurcation) occurs for $\tau < 1$]. As shown in Appendix A, such effects involving maxima pairs do not distinguish trimer dynamics.

A different macroscopic effect happens, however, in the trimer phase space. This is caused by the merging of distinct saddle points (e.g., A_1, A_2) discussed above, that disappear for $\tau > \tau^*$. Since chaotic behavior develops around saddle points, their coalescence should entail an evident local regularization of dynamical behavior.

As a final remark, we wish to observe that state $A_1(-1)$ exhibits the same per-well boson distribution of the ground state. Such two states differ uniquely owing to the phase of the third well. Similarly, state $A_1(0)$ and the π-like state $(\sqrt{N/2}, -\sqrt{N/2}, 0)$ just differ owing to the opposite phase of the second well. Despite their identical boson distribution, such situations will exhibit very different behavior thus confirming the profound influence of the interwell phase differences in distinguishing dynamical states.

IV. CHARACTER OF FIXED POINTS

In this section, we consider the stability character of fixed points just identified. Such a character is recognized by studying the second variation of the energy function on the hypersurface defined by $N = \text{const}$. Explicitly, one should analyze the signature of the quadratic form associated to the Hessian of $\mathcal{H}_3$ (with $N = \text{const}$) in each fixed point. Being this process rather technical, we mainly develop it in Appendix D. Below, after showing how the separation of $\mathcal{H}_3$ in two independent (local) subhamiltonians simplifies remarkably the stability analysis, we summarize the results obtained.

To simplify $\mathcal{H}_3$, it is advantageous to introduce the local variables $\xi_j = z_j - v_j$, where v_j are the coordinates of some given fixed point. Then, neglecting third and fourth order terms, $\mathcal{H}_3$ takes the form

$$\mathcal{H}_3 = \mathcal{H}_3(v) + \sum_{i=1}^{3} (2U|v_j|^2 - \mu - T)|\xi_i|^2 + \sum_{j=1}^{3} U(v_j^* \xi_j + v_j \xi_j^*)^2 + \frac{T}{4} \sum_{i \neq k} |\xi_i - \xi_k|^2, \tag{17}$$

which undergoes the further simplification $v_i = v_i^* \to x_i$ when one recalls that the phase factor of $v_i \in \mathbb{C}$ is a constant that can be absorbed by ξ_j. This fact allows us to separate $\mathcal{H}_3$ in a q-dependent part and a p-dependent part, with $\xi_j := q_j + i p_j$. By making explicit the latter definition in $\mathcal{H}_3$, we find

$$\mathcal{H}_3 = \mathcal{H}_0 + h(q; 6U, T, \mu) + h(p; 2U, T, \mu), \tag{18}$$

where $\mathcal{H}_0 := \mathcal{H}_3(v)$, and

$$h(q; 6U, T, \mu) := \sum_{ij} (M_q)_{ij} q_i q_j, \tag{19}$$

$$h(p; 2U, T, \mu) := \sum_{ij} (M_p)_{ij} p_i p_j. \tag{20}$$

Dynamical matrices M_q and M_p are defined as

$$M_q = -\frac{T}{2} \begin{bmatrix} \Delta_1 & 1 & 1 \\ 1 & \Delta_2 & 1 \\ 1 & 1 & \Delta_3 \end{bmatrix}, \tag{21}$$

$$M_p = -\frac{T}{2} \begin{bmatrix} \delta_1 & 1 & 1 \\ 1 & \delta_2 & 1 \\ 1 & 1 & \delta_3 \end{bmatrix}, \tag{22}$$

with $\Delta_j := 2(\mu - 6Ux_j^2)/T$ and $\delta_j := 2(\mu - 2Ux_j^2)/T$. Hence, the diagonalization of the (local) quadratic form associated to $\mathcal{H}_3$ can be performed in a separate way in Eqs. (19) and (20). Further simplifications come from the fact that matrix M_p is proven to always have a vanishing eigenvalue (see Appendix C), while, due to the conserved quantity $N = \Sigma_i |z_i|^2 = \text{const}$, the induced local constraint $q_1 x_1 + q_2 x_2 + q_3 x_3 = 0$ makes $h(q; 2U, T, \mu)$ dependent only on two variables q_i (see Appendix D).

The stability character for ground states, vortex states, SDW states, and dimerlike states is studied explicitly in Appendix D. The calculation of the $\mathcal{H}_3$ second variation and, when this is necessary, of Hessian eigenvalues provide the following scenario.

(i) States with $x_1 = x_2 = x_3$ are energy minima.

(ii) Vortex configurations are saddle points.

(iii) SDW configurations are saddle points.

(iv) Dimerlike states exhibit two saddle points and one maximum point for $0 < \tau < \tau^*$.

In the last case the merging of the two saddle points to form a regular point is enacted for $\tau \to \tau^*$. Thus, for $\tau^* < \tau$, a single maximum survives.

V. MAPPING OF DYNAMICS ON THE REDUCED PHASE SPACE

We develop a both qualitative and quantitative analysis of the chaotic behavior of the trimer based on the Poincaré section method. After performing a qualitative study of the periodic-orbit instability, we effect a quantitative analysis by measuring the very chaos' indicator, namely, the Lyapunov exponent of every single orbit chosen near a period one. To this end, we introduce a more suitable coordinate system involving a symplectic reduction of dynamics.

Hamiltonian (1) depends on three complex degrees of freedom and commutes with the boson number N. This fact as well as the structure of coupling term in $\mathcal{H}_3$ permit us to reduce from six to four the number of (real) canonical coordinates. The numerical integration of Eqs. (2), thus, furnishes a system picture consisting of a trajectory in a four-dimensional (4D) *reduced* phase-space $\mathcal{P}\in\mathbb{C}^3$. In $\mathcal{P}$, a Poincaré section (PS) is the figure made by the points where a trajectory cut a 2D reference plane. The new set of canonical coordinates used to construct the PS embodies explicitly the conserved quantity $\Sigma_{i=1}^{3}|z_i|^2=N$. Complex coordinates $z_i=\sqrt{n_i}\exp(i\theta_i)$ are replaced by

$$\begin{aligned}&\phi_1=\theta_2-\theta_1, \quad \xi_1=(n_2+n_3-n_1)/N,\\ &\phi_2=\theta_3-\theta_2, \quad \xi_2=(n_3-n_1-n_2)/N,\\ &\psi=(\theta_3+\theta_1)/2, \quad N=n_1+n_2+n_3,\end{aligned} \tag{23}$$

which obey the canonical Poisson brackets

$$\begin{aligned}&\{\phi_i,\xi_j\}=-2\,\delta_{ij}/N, \quad \{\phi_i,N\}=0,\\ &\{\psi,\xi_j\}=0, \quad \{\psi,N\}=-1.\end{aligned} \tag{24}$$

With such new variables [31] $\mathcal{H}_3$ becomes

$$\begin{aligned}\mathcal{E}=\frac{2}{UN^2}\mathcal{H}(\xi_1,\xi_2,\phi_1,\phi_2)&=\mathcal{E}_0+\xi_1^2+\xi_2^2-\xi_1\xi_2-\xi_1+\xi_2\\ &-\tau\sqrt{(1-\xi_1)(\xi_1-\xi_2)(1+\xi_2)}\left[\frac{\cos\phi_1}{\sqrt{(1+\xi_2)}}+\frac{\cos\phi_2}{\sqrt{(1-\xi_1)}}\right.\\ &\left.+\frac{\cos\phi_{12}}{\sqrt{(\xi_1-\xi_2)}}\right],\end{aligned} \tag{25}$$

in which $\phi_{12}:=\phi_1+\phi_2$, $\mathcal{E}_0=1-2\mu/(UN)$ (the associated Hamiltonian equations are contained in Appendix E). In terms of coordinates $(\xi_1,\xi_2,\phi_1,\phi_2)$ the ground-state configuration (4) and vortexlike fixed points (6) correspond to

$$(\tfrac{1}{3},-\tfrac{1}{3},0,0), \quad (\tfrac{1}{3},-\tfrac{1}{3},\tfrac{2}{3}\pi k,\tfrac{2}{3}\pi k)$$

$(k=1,2)$, respectively. Dimerlike fixed points [consider, e.g., A_1 in Eq. (10)] are given by

$$(\xi_1,2\xi_1-1,0,\pi),$$

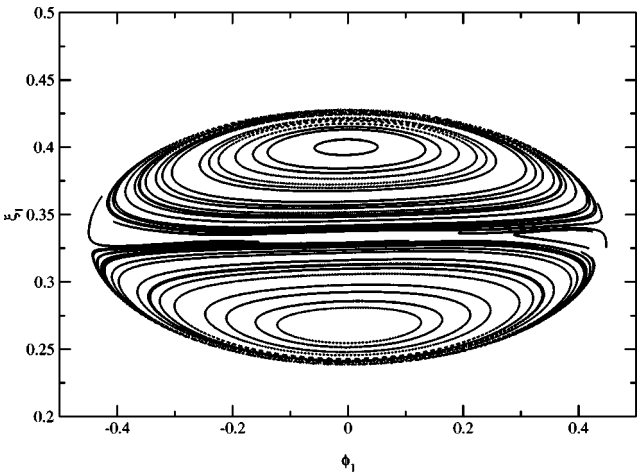

FIG. 1. Poincaré section at $\mathcal{E}\simeq 0.47$ and $\xi_2=-1/3$. In the neighborhood of the ground state, the phase-space trajectories are regular.

where $\xi_1=1-2a_1^2(\tau)/N$ and $a_1(\tau)$ is defined by Eqs. (11), whereas SDW states can be expressed as $(0,0,\varphi,\pi-\varphi)$ for $n_2=0$.

Operationally, the motion equations (2) are numerically integrated by using a first-order bilateral symplectic scheme; the algorithm precision is checked by monitoring the conserved quantities, that is, the system energy and total number of bosons. Trajectories can be traced in the phase space $\mathcal{P}$ in terms of ξ_1, ξ_2, ϕ_1, and ϕ_2. For any given value of the reduced energy, Hamiltonian (25) defines a 3D hypersurface in $\mathcal{P}$. The 2D surface used to construct a PS then is obtained by firming the value of ξ_2 to a constant. Hence, PS is made by coordinates (ξ_1,ϕ_1) of the points' set in which trajectories cut the selected 2D surface.

Discussion of numerical results

We present the results of the numerical analysis aimed at investigating the phenomenology of the trimer dynamics in proximity of fixed points–these identify with the periodic orbits that stationarize $\mathcal{H}_3$ with $N=\text{const}$—calculated in Sec. III. The Hamiltonian parameters chosen for the numerical simulations are

$$\tau=T/NU=0.1, \quad \upsilon=0. \tag{26}$$

Simulations have been carried out by using an integration time step of order 1×10^{-4}, while the total number of time steps employed in constructing each orbit is of order 2^{28}. For each periodic orbit a PS has been selected by setting $\xi_2=\text{const}$, $d\xi_2/dt>0$ and the reduced energy $\mathcal{E}=2E/UN^2=\text{const}$; on this section we have considered samples of about 100 initial conditions (IC). Also, the maximum Lyapunov exponent (MLE) has been measured for each trajectory of the samples associated to the extremal periodic orbits.

Ground state. The PS of this case is fixed by the condition $\xi_2=-1/3$. About 100 initial conditions have been chosen in the $\xi_1-\phi_1$ plane, placed close to the point $(\xi_1,\phi_1)=(1/3,0)$. The energy of the corresponding trajectories is $\mathcal{E}\simeq 0.47$. Figure 1 shows that all the trajectories are regular in

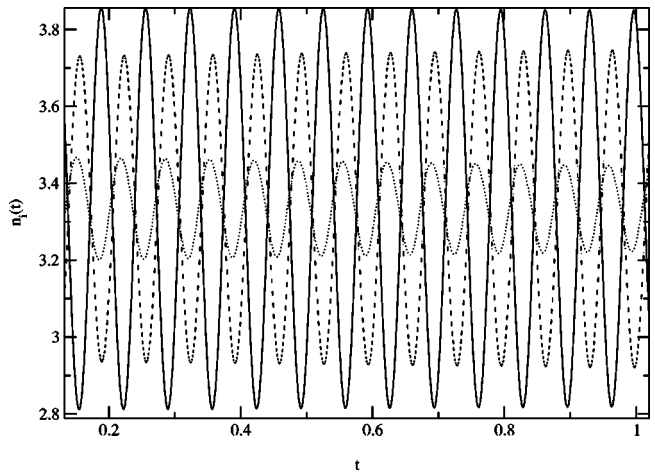

FIG. 2. Typical time evolution of the condensates' populations related to a motion with initial conditions close to a ground-state configuration. The solid, dashed, and dotted lines refer to $n_1(t)$, $n_2(t)$, and $n_3(t)$, respectively. The dynamics appears to be periodic (within the simulation time scale).

the phase space $\mathcal{P}$. Their regular character appears to be consistent with the periodic character shown by the oscillations of populations $n_i=|z_i|^2$ (see Fig. 2) of each condensate.

Vortexlike initial conditions. The choice $\xi_2=-0.3$, $\mathcal{E}\simeq 0.77$ distinguishes the PS of the present case. The initial conditions for the trajectories have been chosen close to the fixed points $(\xi_1,\phi_1)=(1/3,2k\pi/3)$, $k=1,2$ (vortex state). Since no difference distinguishes the PS with $k=1$ and that with $k=2$, we restrict our attention to $k=1$. Figure 3 shows the presence of both regular and chaotic trajectories [Fig. 4 supplies two examples, one for each orbit type]. It shows as well that the PS points related to chaotic trajectories are distributed in a region well separated from that occupied by points generating regular orbits. In particular, the PS displayed in Fig. 3 [together with other PS involving slightly different ξ_2 $(\simeq -1/3)$] suggests that the vortex-state fixed

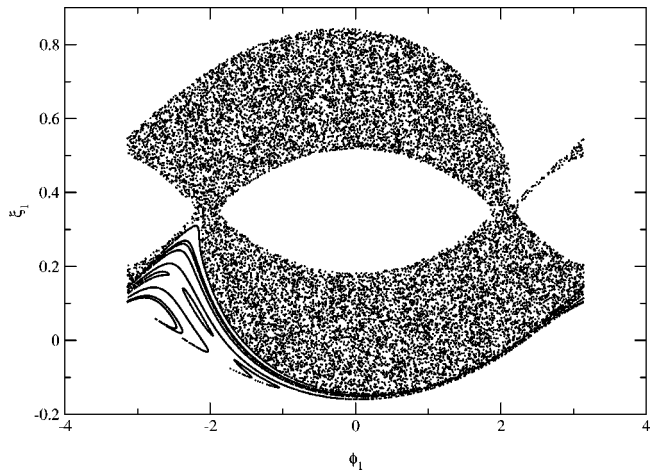

FIG. 3. Poincaré section at $\mathcal{E}\simeq 0.77$ and $\xi_2=-0.3$ for orbits close to a vortexlike fixed point. Even if some regular orbits are present, phase-space trajectories show a dominating chaotic character.

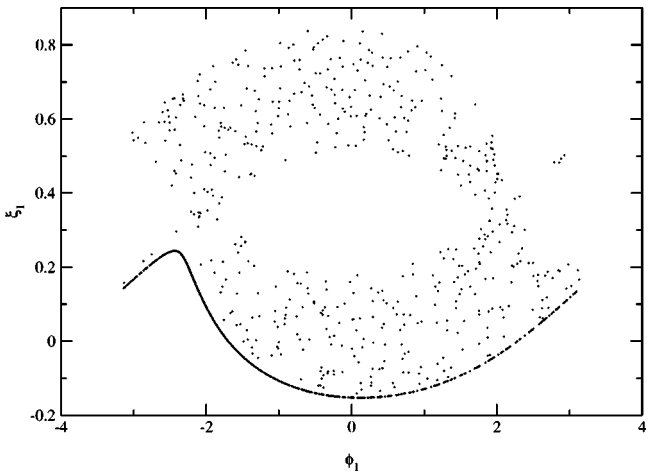

FIG. 4. Representation of a regular orbit (identified by the almost continuous line) and of a chaotic one chosen among those of the PS of Fig. 3.

point is basically surrounded by chaotic orbits. In Fig. 3, to reach the nearest regular orbits starting from $\xi_1=1/3$, $\phi_1=-2\pi/3$, a finite variation of both ξ_1 and ϕ_1 is necessary.

When this change is carried out the trimer-population oscillations change in a significant way. The time evolution of condensate populations n_i $(i=1,2,3)$ related to the nonchaotic orbit of Fig. 4 is illustrated in Fig. 5 and confirms its regular character. By considering IC closer and closer to the vortex-state position such a character is progressively lost. This is shown in Fig. 6 that plots populations n_i, as a function of time, for the chaotic trajectory of Fig. 4.

The regular orbit of Fig. 4 involves an evident *self-trapping* effect provided their IC are enough far from $(\xi_1,\phi_1)=(1/3,-2\pi/3)$. This is clearly manifested in Fig. 5 where $n_i(t)$'s oscillate in such a way that $n_2(t)<n_1(s)$, $n_3(s)$, $\forall\ t$, $\forall\ s$: a *stable gap*, in fact, separates n_2 from n_1, n_3. On the contrary, no stable gap is involved, in general, by chaotic orbits (see Fig. 6) that develop large oscillations on the whole range of n_i. The fact that, in average, $n_i\simeq 1/3$ is

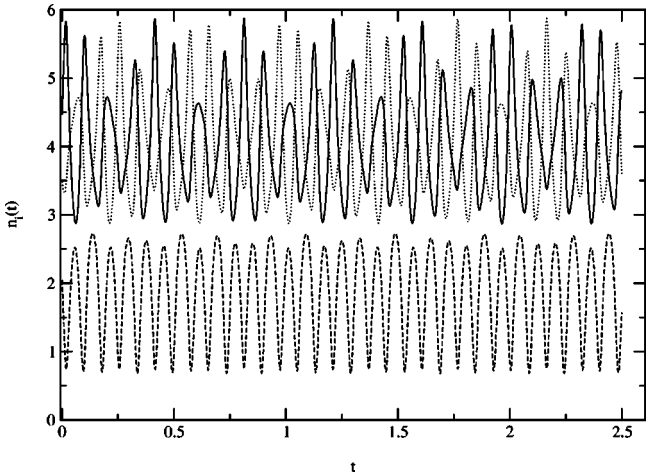

FIG. 5. Time evolution of condensate populations $n_1(t)$ (solid line), $n_2(t)$ (dashed line), and $n_3(t)$ (dotted line) for the regular trajectory of Fig. 4.

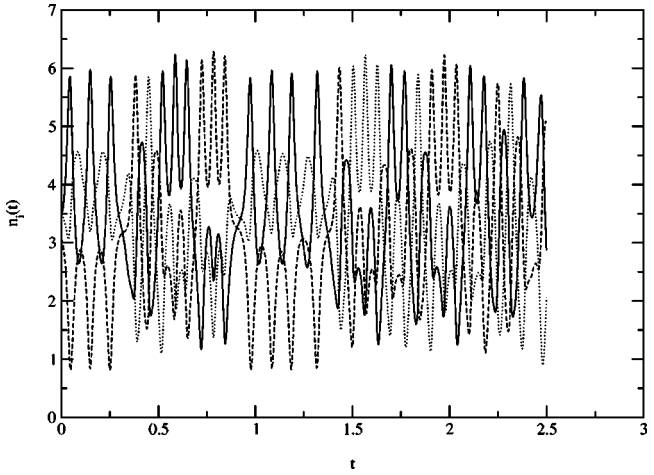

FIG. 6. Populations n_1 (solid line), n_2 (dashed line), and n_3 (dotted line) are plotted as a function of the time for the chaotic trajectory shown in Fig. 4.

the only feature inherited by the vortex state.

SDW-like intial conditions. In this case the choice $\xi_2 = -0.002$ and $\mathcal{E} \simeq 1.09$ fixes the PS that is represented in Fig. 7. The zoom of the section reveals regular trajectories in $\mathcal{P}$ placed near SDW fixed points the latter being characterized by $\xi_2 = 0 = \xi_1$, $\phi_1 = \varphi$, $\phi_2 = \pi - \varphi$, where we have set (φ can be chosen arbitrarily) $\varphi = 0.57\pi$. Figure 8 describes the PS of a chaotic orbit chosen among those of Fig. 7: The PS points are distributed in two, well separated, basins in a quite evident way. The interpretation of such an effect is the following: after recalling that setting $\xi_2 \simeq 0$ implies that $n_3 \simeq 1/2$, one deduces that, concerning the points of the PS, the values allowed for n_1 are either $n_1 \simeq 1/2$ or $n_1 \simeq 0$, which involves either $n_2 \simeq 0$ or $n_2 \simeq 1/2$, respectively.

One therefore recognizes the presence of an *population-inversion* phenomenon between n_1 and n_2. Interestingly, no intermediate values seems to be permitted. The corresponding scenario is given, on a shorter time interval, in Fig. 9 where the nonperiodic oscillations of populations $n_1(t)$, $n_2(t)$, and $n_3(t)$ are compared and a population-inversion

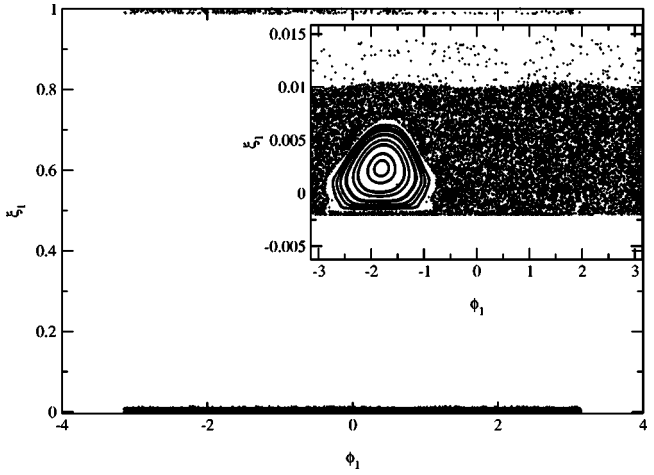

FIG. 7. Poincaré section at $\mathcal{E} \simeq 1.09$ and $\xi_2 = -0.002$ relative to orbits close to a SDW fixed point.

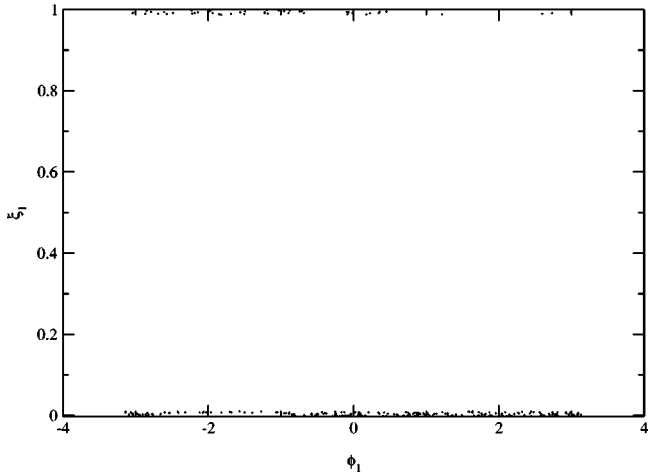

FIG. 8. Representation of one of the chaotic trajectories contained in the Poincaré section of Fig. 7.

effect involving n_1, n_2 gets going. The population oscillations referred to a regular orbit of those contained in the zoom of Fig. 7 are shown in Fig. 10.

Dimerlike initial conditions. As proven in Secs. III and IV, the fixed points of this case consist of two saddle points and a maximum. The conditions $\xi_2 = -0.295$, $\mathcal{E} \simeq 0.73$ and $\xi_2 = -0.005$, $\mathcal{E} \simeq 0.91$ firm the PS associated with the first saddle (see Fig. 11) with coordinates $\xi_1 = -\xi_2 = 0.295$, $\phi_1 = -\phi_2 = \pi$, and to the second saddle (see Fig. 15) with coordinates $\xi_1 = -\xi_2 = 0.005$, $\phi_1 = -\phi_2 = \pi$, respectively. In both the cases, the PSs exhibit both regular and chaotic trajectories. Concerning Fig. 11 (first saddle point), the coexistence of such regimes is confirmed in Fig. 12, where the PS of a regular trajectory is compared with the PS of a chaotic one (see also Figs. 13 and 14). Figure 16 shows analogous quantities referred to the second saddle point. It is worth noting that in the latter case the neighborhood of the saddle point is characterized IC issuing regular orbits, whereas the first saddle is surrounded by IC generating chaotic motions.

In Fig. 15, regular orbits reside either on the bottom or on

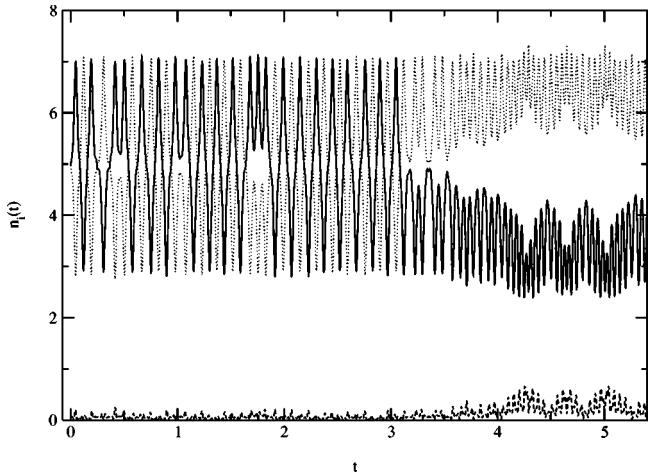

FIG. 9. The figure plots the populations $n_1(t)$ (solid line), $n_2(t)$ (dashed line), and $n_3(t)$ (dotted line), as a function of the time, for the chaotic trajectory shown in Fig. 8.

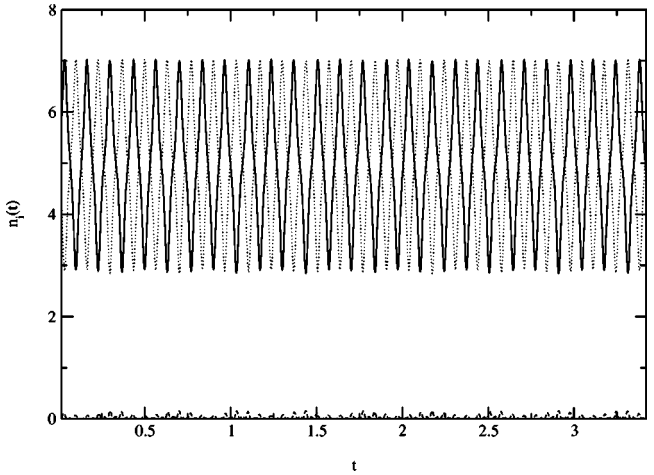

FIG. 10. Populations of the three condensates: n_1 (solid line), n_2 (dashed line), and n_3 (dotted line) as a function of the time for a regular trajectory of the zoom shown in Fig. 7.

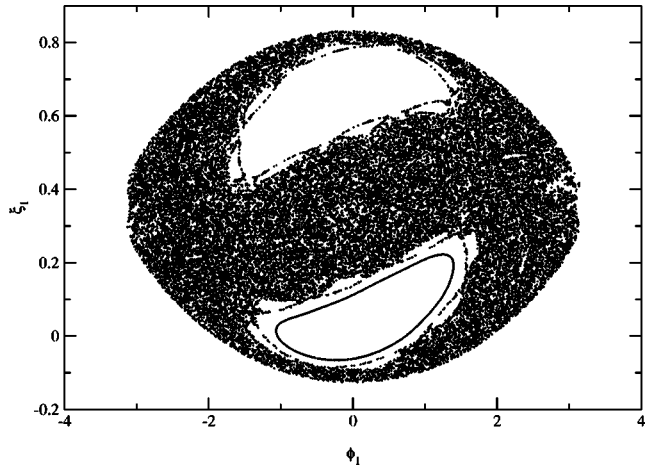

FIG. 11. Poincaré section firmed by the conditions $\xi_2 = -0.295$ and $\mathcal{E} \simeq 0.73$, close to a dimerlike (saddle) fixed point.

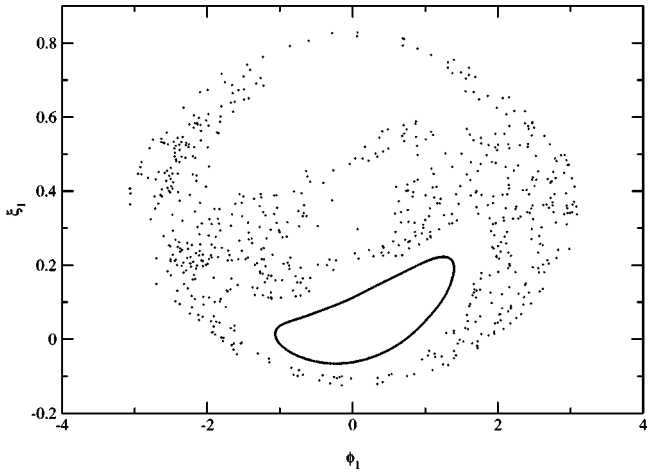

FIG. 12. This figure shows a regular trajectory and a chaotic one chosen among those of Fig. 11.

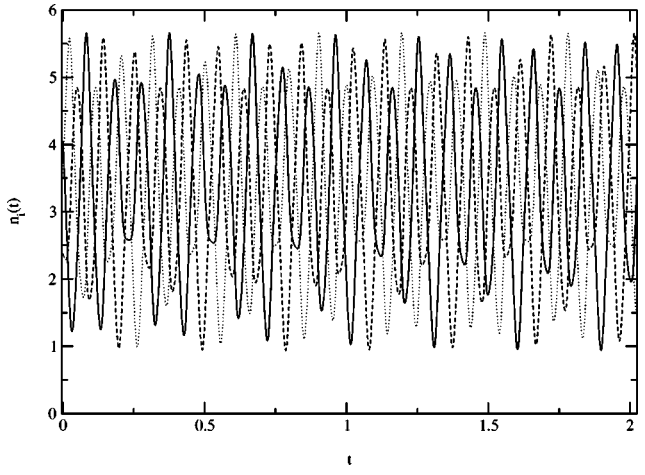

FIG. 13. Temporal behavior of the condensates' populations related to the regular trajectory of Fig. 12. The solid, dashed, and dotted lines refer to $n_1(t)$, $n_2(t)$, and $n_3(t)$, respectively.

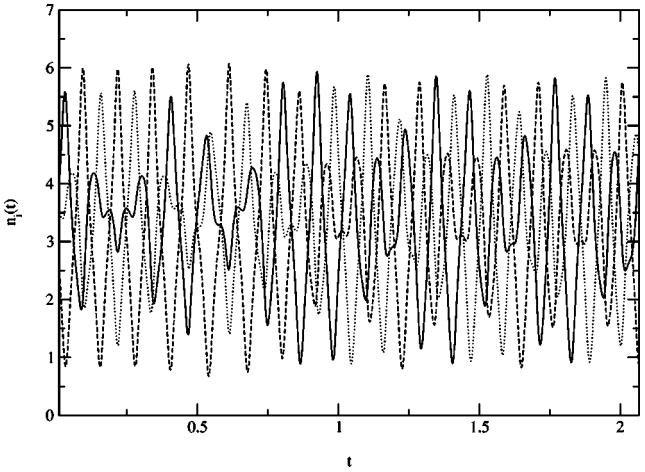

FIG. 14. Condensates' populations, as a function of the time, related to the chaotic trajectory of Fig. 12. The solid, dashed, and dotted lines refer to $n_1(t)$, $n_2(t)$, and $n_3(t)$, respectively.

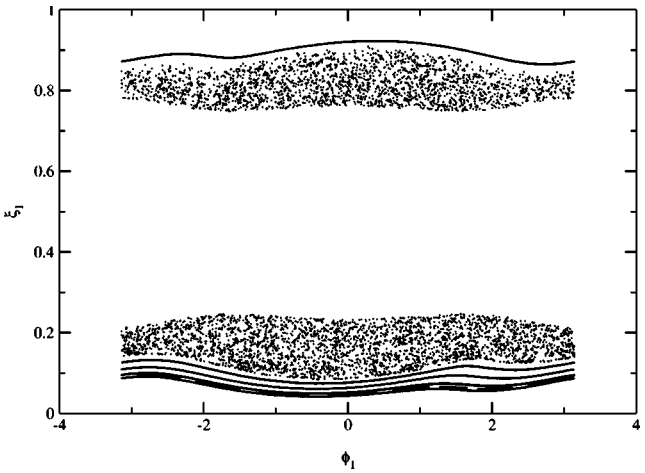

FIG. 15. Poincaré section firmed by the conditions $\xi_2 = -0.005$ and $\mathcal{E} \simeq 0.91$, close to a saddle dimerlike fixed point.

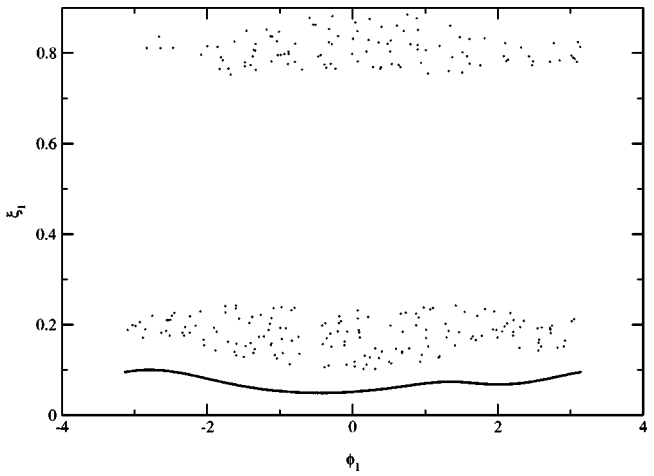

FIG. 16. This figure shows a regular trajectory and a chaotic one chosen among those of Fig. 15.

the top of the figure, but dynamics never connects the top orbits with the bottom ones. This feature is confirmed by the time behavior (see Fig. 17) of $n_i(t)$ related to the regular trajectory of Fig. 16. In Fig. 17, the presence of the gap between $n_2(\simeq 0.5)$ and n_1, n_3 $(\simeq 5)$ indicates a macroscopic self-trapping effect. The latter differs from the dimerlike self-trapping reviewed in Sec. II A, where $z_1 = z_3 \rightarrow n_1 = n_3$, in that n_1, n_3 develop *independent* oscillations. The scenario just described no longer holds for the chaotic orbits: Figure 18 shows an *intermittent* effect of population inversion between n_1 and n_2. This reflects the fact the points of the chaotic orbit of Fig. 16 are distributed intermittently both in the higher and in the lower part of the PS.

The trajectories near the maximum (we consider the case $\xi_1 = 0.999$, $\xi_2 = 0.998$, $\phi_1 = -\phi_2 = \pi$,) appear to be regular, as one can deduce from Fig. 19 that shows PS close to a maximum fixed point with $\xi_2 = 0.8$ and $\mathcal{E} \simeq 1.7$. In this case, populations $n_1(t)$, $n_2(t)$, and $n_3(t)$ display in Fig. 20 a periodic effect of *population-inversion* involving n_1, n_2, whereas the fact that $n_1, n_2 \ll n_3$ entails an evident self-trapping phenomenon.

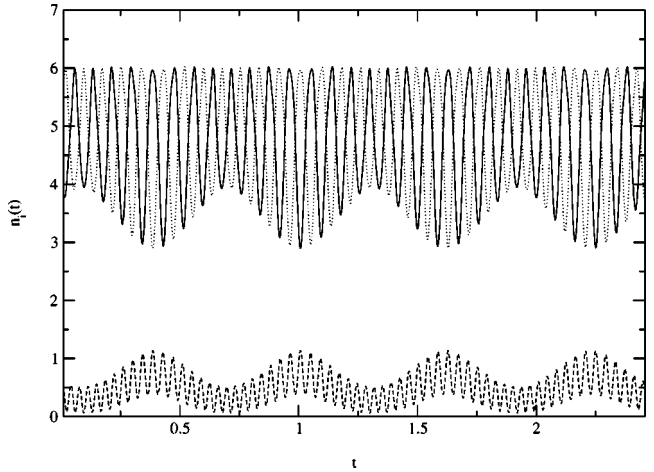

FIG. 17. Temporal behavior of the condensates' populations related to the regular trajectory of Fig. 16. The solid, dashed, and dotted lines trace $n_1(t)$, $n_2(t)$, and $n_3(t)$, respectively.

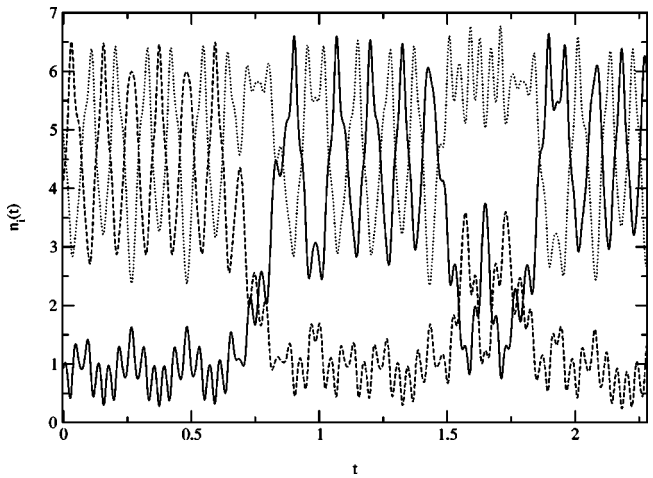

FIG. 18. Condensates' populations, as a function of the time, related to the chaotic trajectory of Fig. 16. The solid, dashed, and dotted lines trace $n_1(t)$, $n_2(t)$, and $n_3(t)$ respectively.

The averages of the MLEs calculated for the chaotic orbits are 0.74 (Fig. 3), 0.42 (Fig. 7), 0.29 (Fig. 11), and 0.96 (Fig. 15). The evaluation of the MLE for the regular trajectories described in the previous examples (as well as for those of Fig. 1 and Fig. 19) exhibit the expected decreasing behavior thus suggesting that a weak stochastic feature occurrs on such trajectories. It is worth mentioning that the analysis of regular and chaotic motions in the Eqs. (2) could be performed quantitatively within a recently proposed geometrical framework to tackle Hamiltonian chaos [20,21]. In particular, a system described by a Hamiltonian quartic in the momenta (which is thus of the same type of the trimerlike one) would require the use of Finsler spaces [22]. Such an interesting possibility is under active consideration.

VI. CONCLUSIONS

In this paper, we have focused our attention on the structure of the phase space of ''classic'' trimer, that is, the mean-

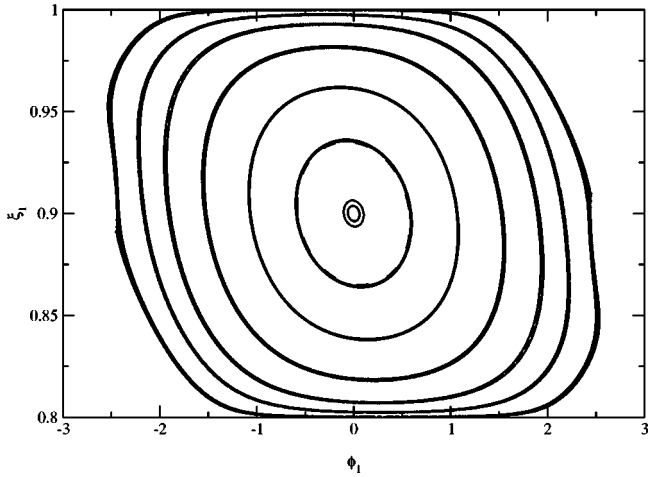

FIG. 19. Poincaré section near a maximum at $\mathcal{E} \simeq 1.7$ and $\xi_2 \simeq 0.8$. In the neighbourhood of the maxima the phase space trajectories are regular.

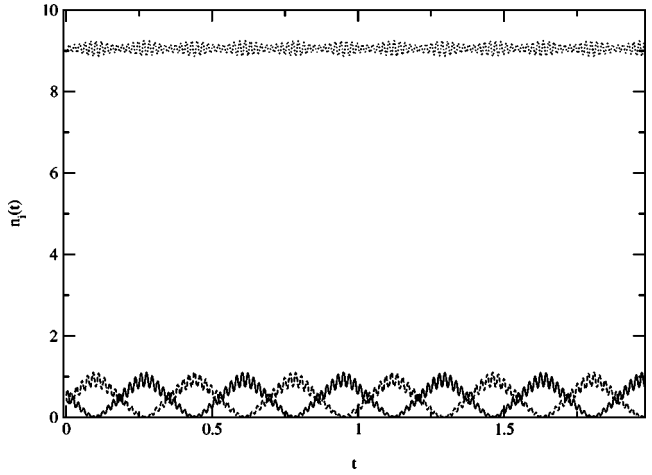

FIG. 20. Time evolution of the condensates' populations related to a motion with initial conditions close to a maximum state configuration. The figure shows $n_1(t)$ (solid line), $n_2(t)$ (dashed line), and $n_3(t)$ (dotted line). The motion appears to be regular.

field form of the model describing three interacting BECs. Our analysis puts in light, on the one hand, the remarkable complexity that characterizes the trimer dynamics (by comparison with the integrable dynamics of the dimer system), on the other hand, the phenomena that are expected to characterize the *M*-well chain of interacting condensates. In view of the recent experimental results, the phenomenology of this system seems more and more viable to experimental observations. Trimer dynamics has been investigated within a semiclassical Hamiltonian picture, reviewed in Sec. II and developed in previous papers, based on a coherent-state representation of the trimer quantum state.

The identification of the set of fixed points of trimer Hamiltonian equations and the fact that such points are associated to periodic solutions (collective modes) of several types represents the initial, central result of our paper. The presence of the constraint $N=\text{const}$ entails that the states that stationarize the Hamiltonian are not isolated points but periodic orbits (one-dimensional manifolds). The solutions thus found enlarge the set of exact solutions [11,13] pertaining the dimerlike integrable subregimes of trimer and exhibiting a parameter-dependent self-trapping effect.

Based on the second variation (with $N=\text{const}$) of the energy function around its fixed points, the character of the latter has been recognized in Sec. IV and Appendix D thereby revealing the presence of several saddle points and maxima, in addition to the expected ground state. Numerical simulations and the PS method have furnished a wide scenario of trimer dynamical behaviors whose possible *chaotic* character has been tested by measuring the maximum Lyapunov exponent. We summarize the results of our dynamical simulations.

(i) The orbits that have ICs close to ground-state exhibit a regular behavior with periodic oscillations of populations n_i.

(ii) On the contrary, orbits with vortexlike IC (namely, based at points close to vortex fixed points) are, in general, chaotic. Regular orbits, however, are found at sufficient distance from vortex fixed points. For such orbits a stable gap separates the oscillations of n_i from those of n_j, n_k $(j,k \neq i)$ thus generating self-trapping; n_j, n_k show independent oscillations (in Sec. VI configurations with $i=2$, $j=1$, $k=3$ has been considered). The gap disappears for chaotic orbits.

(iii) Orbits with SDW-like ICs also display both regular and chaotic behaviors but their ICs are not separated spatially. The regular orbits we have considered keep the memory of the IC since one of the three wells remains almost empty (pure dimer) while the other two undergo regular oscillations. Such states identify essentially with π-like states and manifest a stable character. An example of *chaos emergence*, which starts with a macroscopic population inversion entailing the filling of the (initially) depleted well, has been detected by assuming various SDW-like ICs involving chaotic orbits.

(iv) Regular orbits generated by dimerlike ICs (related to the second saddle point) exhibit periodic oscillations of n_i's with an evident self-trapping. Chaotic orbits, instead, give rise to oscillations displaying self-trapping on short-time intervals and *intermittent* population-inversion effects. ICs close to the maxima further generate regular orbits with self-trapping. The corresponding states display the presence of a unique almost filled well [23].

The scenario just depicted supplies a rich account of properties, behaviors and possible observable effects issuing from trimer dynamics and suggests promising future developments.

We emphasize the fact that $\tau=T/NU$ is the parameter that actually characterizes the dynamical behavior and that the changes of τ can be caused by varying *U*, *T*, and *N*. While the ground state, the vortex states, and the SDW states [see Eqs. (4), (6), and (8), respectively] have been shown to be τ independent, dimerlike fixed points have revealed a complex dependence on τ. The interesting result of Sec. III D is that for $\tau<\tau_*$ one finds two distinct saddles $A_1(q_1)$, $A_2(q_2)$ and a maximum $A_3(p)$ [such configurations are defined explicitly via Eqs. (10)–(13), while the τ-dependent parameters q_1, q_2, and p were derived in Appendix B], whereas, for $\tau>\tau_*$, only the $A_3(p)$ survives. This effect might have a macroscopic character since the A_1-A_2 coalescence for $\tau=\tau_*$ is expected to cause chaos suppression (see Sec. III D).

The basic configurations (ground state, vortex states, SDW states, and dimerlike states involving both saddle and maximum points) recognized in the present work, and the complexity of dynamical regimes, both chaotic and regular, that develop in their neighborhoods deserve further investigations in two directions at least. First, classically, one should carry out a systematic study (requiring huge computational resources) of long-time behavior of dynamical states of interest to disclose further macroscopic effects. For the same reason, a larger number of ICs (together with the trajectories thus issued) should be considered near fixed-point configurations.

We point out the fact that predictions on the dynamics of phases ϕ_i should be important in relation to phase-interference experiments [3]. This aspect, which has not been deepened in the present work, requires a separate analysis and further numerical study directed to detect phenomena

exhibiting phase coherence and their stability in proximity of states endowed with ordered phase configurations such as vortex states ($\phi_i = 2\pi k/3$, $k=1,2$), SDW states ($\phi_i - \phi_j = \pi$, $i \neq j$, $|z_k| = 0$ with $i,j \neq k$), and dimer configurations ($\phi_i = \phi_j$, $z_k \neq z_i = z_j$ with $i,j \neq k$).

Second, in view of the possibility of realizing systems with small per-well populations, the pure quantum approach to trimer dynamics (along the same lines of previous work directed to study the spectral properties of dimer) seems to be quite natural [32]. The study of quantum trimer might put in evidence unexpected effects caused by the competition of chaotic (classical) behavior and integrable (quantum) behavior on the borderline of appropriate mesoscopic regimes where the transition from quantum to classical dynamics takes place.

ACKNOWLEDGMENTS

We are indebted to P. Buonsante for his comments. The work of V.P. has been supported by INFM (Italy) and MURST (within the Project ''Theory of Coherent Fluids''). R.F. gratefully acknowledges the financial support of MURST (within the Project ''Complex Problems in Statistical Mechanics and Field Theory'') and INFN (Italy), as well as Professor E. Arimondo and his group for useful discussions.

APPENDIX A: DERIVATION OF FIXED POINTS

Equations (3) can be simplified by noting their invariance under the global symmetry transformation $z_\ell \to z_\ell \exp(i\Phi)$ and the fact that $z_\ell / Z \in \mathbb{R}$ (whenever $Z \neq 0$) with $\ell = 1,2,3$. Then one can set $z_\ell \equiv x_\ell \exp(i\Phi)$, where the x_ℓ are real numbers and Φ is an arbitrary phase, thus reducing Eqs. (3) to a system of the three real equations

$$E_j(\mathbf{x}) := \left(2Ux_j^2 - \mu + \frac{T}{2} \right) x_j - \frac{T}{2} X \equiv 0, \tag{A1}$$

with $j=1,2,3$ and $X := x_1 + x_2 + x_3$. When the condition $x_i \neq 0$ for $i=1,2,3$ is imposed, the latter equations can be recast in terms of an equivalent system of three equations one of which fixes the Lagrange multiplier μ, while the other two, now formulated in a μ-independent form, determine x_1, x_2, x_3 thanks to the further condition $N = \text{const}$. In fact, the sum of the quantities $E_j(\mathbf{x})/x_j$ can be set equal to zero provided $x_j \neq 0$ thus giving the equation

$$3\mu = 2UN - \frac{T}{2} \sum_i \frac{X - x_i}{x_i}. \tag{A2}$$

Moreover, from $E_1(\mathbf{x})/x_1 - E_2(\mathbf{x})/x_2 = 0$ and $E_3(\mathbf{x})/x_3 - E_2(\mathbf{x})/x_2 = 0$ one obtains

$$0 = (x_2 - x_1) \left[2U(x_2 + x_1) + \frac{TX}{2x_1 x_2} \right], \tag{A3}$$

$$0 = (x_2 - x_3) \left[2U(x_2 + x_3) + \frac{TX}{2x_3 x_2} \right], \tag{A4}$$

completed by the condition $N = x_1^2 + x_2^2 + x_3^2$.

APPENDIX B: DERIVATION OF DIMERLIKE FIXED POINTS

Because of the identification $x_1 = x_2$ (characterizing dimerlike fixed points), Eqs. (A3) and (A4) become a unique equation that can be written as

$$2U(x_1^2 - x_3^2) = \frac{T}{2} \left[1 + \frac{x_3}{x_1} - 2\frac{x_1}{x_3} \right]. \tag{B1}$$

Such an expression suggests two possible ways to parametrize x_1, x_3,

$$\begin{aligned} x_1 &= \sqrt{N} R \cosh\alpha, \quad & x_3 &= \sqrt{N} R \sinh\alpha, \\ x_1 &= \sqrt{N} R \sinh\beta, \quad & x_3 &= \sqrt{N} R \cosh\beta, \end{aligned} \tag{B2}$$

both allowing for the elimination of N in the constraint $2x_1^2 + x_3^2 \equiv N$. They also provide two independent class of solutions that make explicit the three roots involved by the cubic character of Eq. (B1). In the first case, one finds

$$R^2 = \frac{1 - q^2}{2 + q^2}, \quad R^2 = \frac{\tau}{4} \left[1 + q - \frac{2}{q} \right] \tag{B3}$$

[the first formula comes from the constraint on the total number of bosons, the second one comes from Eq. (B1)], whereas the second choice gives

$$R^2 = \frac{1 - p^2}{1 + 2p^2}, \quad R^2 = \frac{\tau}{4} \left[2p - 1 - \frac{1}{p} \right], \tag{B4}$$

where $\tau := T/UN$, $q = \tanh\alpha$, $p = \tanh\beta$, and $\alpha, \beta \in \mathbf{R}$. System (B3) reduces to the cubic equation

$$\tau(2 + q^2)(2 + q) + 4q(1 + q) = 0, \tag{B5}$$

which, provided $q \in [-1, +1]$ in order to ensure the condition $R^2 \geqslant 0$, supplies either two or none solutions, depending on the fact that $\tau < \tau_*$, $\tau > \tau_*$. By solving the system one finds that the two roots $q_\nu(\tau)$, $\nu = 1,2$ range in $[-1,0]$ and fulfil the conditions

$$-1 \leqslant q_1 \leqslant q_2 \leqslant 0 \quad \text{for} \quad 0 \leqslant \tau \leqslant \tau^*,$$

with $q_1(\tau) = q_2(\tau)$ for $\tau = \tau^*$. The parameter τ_* is identified by imposing, in addition to Eq. (B5), the requirement that the two q-dependent functions of Eqs. (B3) (that is, the two right-hand sides) be tangent at some point,

$$\frac{-6q}{(2 + q^2)^2} \equiv \frac{\tau}{4} \left[1 + \frac{2}{q^2} \right]. \tag{B6}$$

Equations (B5) and (B6), solved numerically, supply the value $\tau^* \simeq 0.297\,18$.

Such a structure does not characterize system (B4), which always exhibits a single solution for some appropriate value in the sector $p \in [-1/2, 0]$ obtained from the equation

$$\tau(1+2p^2)(1+2p)+4p(1+p)=0. \tag{B7}$$

In view of the restriction $q,p<0$, from definitions (B2) one deduces that the fixed-point coordinates are such that $x_1x_3<0$. The three solutions $q_1(\tau)$, $q_2(\tau)$, $p(\tau)$ just obtained correspond, within the space of coordinates $\{(x_1,x_2,x_3)\}\equiv\mathbf{R}^3$, to three vectors expressed as

$$\begin{aligned} A_1&:=(a_1,a_1,-(a_1/|a_1|)\sqrt{N-2a_1^2}),\\ A_2&:=(a_2,a_2,-(a_2/|a_2|)\sqrt{N-2a_2^2}),\\ A_3&:=(a_3,a_3,-(a_3/|a_3|)\sqrt{N-2a_3^2}), \end{aligned} \tag{B8}$$

where

$$a_3=\pm\left[\frac{Np^2}{1+2p^2}\right]^{1/2},\quad a_\nu=\pm\left[\frac{N}{2+q_\nu^2}\right]^{1/2}, \tag{B9}$$

with q_ν, p solving Eqs. (B5) and (B7). One can easily check that the two τ-dependent curves A_1 and A_2 can be seen as two branches of a unique curve based at the common point $A_1(q_1)=A_2(q_2)$ for $\tau=\tau^*$, where they join smoothly.

Dimerlike fixed points become nine when considering the further set of points generated by index permutations

$$\begin{aligned} B_1&:=(a_1,-(a_1/|a_1|)\sqrt{N-2a_1^2},a_1),\\ B_2&:=(a_2,-(a_2/|a_2|)\sqrt{N-2a_2^2},a_2),\\ B_3&:=(a_3,-(a_3/|a_3|)\sqrt{N-2a_3^2},a_3),\\ C_1&:=(-(a_1/|a_1|)\sqrt{N-2a_1^2},a_1,a_1),\\ C_2&:=(-(a_2/|a_2|)\sqrt{N-2a_2^2},a_2,a_2),\\ C_3&:=(-(a_3/|a_3|\sqrt{N-2a_3^2},a_3,a_3), \end{aligned} \tag{B10, B11}$$

related to the subcases $x_1=x_3\neq x_2$ and $x_3=x_2\neq x_1$. Such nine curves become actually six. Our previous observation on considering A_1 and A_2 as a unique curve, in fact, readily extends the curves B_1, B_2, and C_1, C_2. Due to the double choice $\pm$ in Eq. (11) such curves are 12.

In order to visualize the dimerlike fixed points, one can plot their position vectors A_ℓ, B_ℓ, C_ℓ, $\ell=1,2,3$ within the three-dimensional space by varying their parameters a_ℓ ($\ell=1,2,3$) in the appropriate range. As noted above, in the case $\tau<\tau^*$, for q ranging in the interval $[-1,0]$, Eq. (B5) exhibits its two solutions, whereas, for any τ, Eq. (B7) admits one solution with $p\in[-1/2,0]$. The corresponding ranges of variation for a_ν ($\nu=1,2$) and a_3 are

$$\sqrt{\frac{N}{3}}\leqslant|a_\nu|\leqslant\sqrt{\frac{N}{2}},\quad 0\leqslant|a_3|\leqslant\sqrt{\frac{N}{6}},$$

respectively. The representation of the position of dimerlike fixed points on the sphere $\Sigma_i x_i^2=N$ provides arcs that never intersect the one with the other when τ ranges in $[0,\infty]$. The double sign $\pm$ in parametrizations (B9) entails that each curve P_j ($P=A,B,C$) is formed by two disjoint curves. For P_3 ($P=A,B,C$) one has

$$a_3\in[-\sqrt{N/6},0[,\quad a_3\in]0,\sqrt{N/6}],$$

while for P_1 and P_2 ($P=A,B,C$) the two disjoint branches are originated by the mappings $a_\nu\to P_\nu$ with

$$a_\nu\in[-\sqrt{N/2},-\sqrt{N/3}],\quad a_\nu\in[\sqrt{N/3},\sqrt{N/2}].$$

APPENDIX C: DIAGONALIZATION OF M_p

The diagonalization process of M_p allows one to prove that one of the eigenvalues is always zero. From the standard condition $\det(M_p-\lambda)=0$, one obtains the eigenvalue equation (upon introducing $\Lambda:=2\lambda/T$)

$$\Lambda^3+\left(\sum_j\ \delta_j\right)\Lambda^2+(\delta_1\delta_2+\delta_2\delta_3+\delta_3\delta_1-3)\Lambda+\delta_1\delta_2\delta_3+2-\sum_i\ \delta_i=0, \tag{C1}$$

where $\delta_1\delta_2\delta_3+2-\Sigma_j\delta_j$, upon setting $\delta_j\equiv-(x_\ell+x_k)/x_j$ owing to Eqs. (A1), can be shown to vanish in virtue of the identity

$$\prod_j^*\ (x_\ell+x_k)/x_j=2+\sum_j^*\ (x_\ell+x_k)/x_j.$$

The superscript symbol * recalls that the indices ℓ, k, and j must differ the one from the other. Hence, as a general result, the diagonalization of M_p entails the presence of a zero eigenvalue consistent with the analysis of dynamics in the reduced phase space, developed in Sec. V. In view of the matrix-trace invariance, one also finds

$$\begin{aligned} \sum_{j=1}^3\ \lambda_j&=-\frac{T}{2}\sum_{j=1}^3\ \delta_j\to\lambda_1+\lambda_2\\ &\equiv\frac{T}{2}\sum_j\ \frac{x_\ell+x_k}{x_j}(\equiv-3\mu+2UN), \end{aligned}$$

while the two roots

$$\lambda_\nu=\frac{T}{4}[-\Delta\pm\sqrt{(\Delta)^2-4(\Delta_{123}-3)}], \tag{C2}$$

where, $\Delta=\Sigma_i\delta_i$ and $\Delta_{123}:=\Sigma_i\delta_1\delta_2\delta_3/\delta_i$, and $\nu=1,2$, [λ_1 (λ_2) is joined to $-$ ($+$) in Eq. (C2)], issue from the quadratic equation that emerges from Eq. (C1) when removing a factor Λ.

APPENDIX D: FIXED POINT CHARACTER

This appendix is devoted to recognizing, case by case, the minima, the maxima, and the hyperbolic points within the four (class of) states identified as fixed points. Concerning the eigenvalues of matrix M_q one must take into account the

restriction on the displacements ξ_i from v_i induced by the constraint $N=\Sigma_i|z_i|^2=\text{const}$. After recalling that the phase of v_i can be absorbed, for each i, by ξ_i due to its arbitrariness, the substitution $v_i \to x_i$ implies that

$$N=\sum_i |\xi_i+x_i|^2=\sum_i [|\xi_i|^2+2q_i x_i+x_i^2],$$

which, in turn, entails $\Sigma_i|\xi_i|^2+2q_i x_i=0$, namely—to first order—the plane equation $q_1x_1+q_2x_2+q_3x_3=0$. It represents the restriction on the displacements that variables ξ_i's are allowed to effect. Substituting q_i with $q_i=-(x_r q_r+x_s q_s)/x_i$, where $r,s\neq i$ (and the choice of i depends, in general, on the condition $x_i\neq 0$) finally gives

$$h(q;6U,T,\mu)\equiv\left[2\frac{x_r x_s}{x_i^2}(6Ux_i^2-\mu)+\frac{T(x_r+x_s-x_i)}{x_i}\right]q_r q_s + \sum_{j\neq i}\left[12Ux_j^2-\frac{\mu}{x_i^2}(x_i^2+x_j^2)+T\frac{x_j}{x_i}\right]q_j^2. \tag{D1}$$

1. Ground-state case

These fixed points are characterized by the fact that $x_j=\pm\sqrt{N/3}$ for $j=1,2,3$, and $\mu=2UN/3-T$. By inserting this solutions in Eq. (18) one obtains the Hamiltonian written as

$$\mathcal{H}_3=E_{gs}+\sum_{j=1}^{3}\left[\left(\frac{4}{3}UN+T\right)q_j^2+Tp_j^2\right]-\frac{T}{2}\times\sum_{i\neq j=1}^{3}(p_ip_j+q_iq_j),$$

where E_{gs} is the ground-state energy defined previously. Then, by taking the constraint $N=\Sigma_{j=1}^3|z_j|^2$ into account, one obtains $\Sigma_{j=1}^3[q_j^2+p_j^2\pm 2\sqrt{N/3}q_j]=0$. For little displacements from $q_j=0=p_j$ the latter equation reduces to $\Sigma_{j=1}^3 q_j=0$, which implies that

$$\mathcal{H}_3\simeq E_{gs}+\left(\frac{8}{3}UN+3T\right)(q_1^2+q_2^2+q_1q_2)+T\sum_{i=1}^{3}p_i^2-\frac{T}{2}\sum_{i\neq j=1}^{3}p_ip_j. \tag{D2}$$

The eigenvalues of the Hessian corresponding to the q-dependent and the p-dependent part of $\mathcal{H}_3$ are $\{(3\tau+8/3)UN/2,(9\tau+8)UN/2\}$ and $\{0,3T/2,3T/2\}$, respectively. They are positive, coherent with the fact this is a minimum.

2. Vortex case

The conditions $|x_i|^2=N/3$ and $\mu=(4NU+3T)/6$ characterize vortex configurations. One thus finds

$$h(p;2U,T,\mu)=-T(p_1+p_2+p_3)^2/2<0,$$

whereas from Eq. (D1) one gets

$$h(q;6U,T,\mu)=8UN(q_1^2+q_2^2+q_1q_2)/3>0,$$

whose eigenvalues are always positive. Vortex configurations are therefore saddle points.

3. SDW case

The previous analysis shows that the (fixed point) configurations in which one of the three well is depleted (e.g., well $i=2$) is such that $x_2=0$, $x_1=-x_3=\pm\sqrt{N/2}$ (π-state structure), and $\mu=NU+T/2$. Site index permutations allows one to obtain two further, similar cases. In these points, Hamiltonian (18) can be written as

$$\mathcal{H}_3=E_{dw}+UN[2(q_1^2+q_3^2)-q_2^2]-\frac{T}{2}\left[\left(\sum_{i=1}^{3}q_i\right)^2+\left(\sum_{i=1}^{3}p_i\right)^2\right].$$

In this case, the constraint on the total number of particles supplies the constraint $\Sigma_{j=1}^3(p_j^2+q_j^2)\pm\sqrt{2N}(q_1-q_3)=0$, which reduces to $q_1-q_3\simeq 0$ when $q_j,p_j\simeq 0$. Then $\mathcal{H}_3$ takes the form

$$\mathcal{H}_3\simeq E_{dw}+UN(4q_1^2-q_2^2)-UNp_2^2-\frac{T}{2}[(2q_1+q_2)^2+(p_1+p_2+p_3)^2], \tag{D3}$$

whose Hessian matrix is endowed with the eigenvalues $\{(6-5\tau\pm\sqrt{5(20-12\tau+5\tau^2)})UN/4\}$ and $\{0,-(2+3\tau\pm\sqrt{4-4\tau+9\tau^2})UN/4\}$ for the q-dependent part and the p-dependent part, respectively. The analysis of the signature of such eigenvalues leads to identify the fixed points of the empty-well case with saddle points.

4. Dimerlike case

In the dimerlike case, the conditions on the coordinates are $x:=x_1=x_2\neq x_3=:y$ (none vanishing). Furthermore, one has to impose the condition $(2Ux_j^2-\mu)x_j=T/2\Sigma_{k\neq j}x_k$ on the Lagrange multiplier μ that becomes

$$\mu=[2UN-T(1+y/x+x/y)]/3. \tag{D4}$$

Let us start by analyzing the Hessian eigenvalues of Hamiltonian p sector, namely, of Eq. (20). These eigenvalues are given by Eq. (C2) and one has that whenever the term $\sigma:=(\delta_1\delta_2+\delta_2\delta_3+\delta_3\delta_1-3)$ is greater then zero, these eigenvalues are negative. To verify the condition $\sigma>0$ one can proceed in the following way. First, one substitutes in σ the δ_j written in term of their definitions; namely, in term of μ, T, U and the fixed-points coordinates x,y, Second, one writes μ in terms of x, y and, etc. [Eq. (D4)]. Finally, one eliminates the dependence on x, y, and T in σ by choosing either the parametrization

$$y/x=q, \quad x=\pm\sqrt{N/(2+q^2)},$$

combined with Eq. (B5) to express the q dependence of τ, or the parametrization

$$x/y=p, \quad x=\pm\sqrt{Np^2/(1+2p^2)},$$

combined with Eq. (B7) to express the p dependence of τ. The expression for σ achieved in such a way depends on q or p, respectively. One can show that both the expressions are always positive in the range of definition of q ($[-1,0]$) and p ($[-1/2,0]$), which means that eigenvalues (C2) are all negative.

As usual, for working out the Hessian eigenvalues of Hamiltonian (19) related to the q part of the original one, it is necessary to take into account the constraint $\Sigma_i|z_i|^2=N=\text{const}$. The latter, in the present case, becomes $q_3\equiv-(q_1+q_2)x/y$. By means of this condition, one can reduce the dimension of the eigenvalues problem related to Eq. (19) from 9 to 4. The Hamiltonian $h_r(q_1,q_2,U,\mu,T)$ thereby obtained can be further simplified via the substitutions $\mu\rightarrow\mu=[2UN-T(1+y/x+2x/y)]/3$ and $y/x=q$ or $x/y=p$, depending on the parametrization one adopts. With the first choice ($y/x=q$), and relying on Eq. (B5), one finds two Hessian eigenvalues one of which is always positive, while the other has an ill-defined sign in the domain $q\in[-1,0]$. By using the second parametrization $x/y=p$ and Eq. (B7), both the eigenvalues thus obtained can be proven to be negative for $p\in[-1/2,0]$. In summary, in the dimerlike case, for $0<\tau<\tau^*$, one has two saddle points and one maximum point; for $\tau^*<\tau$, instead, fixed points reduce to a single maximum point.

APPENDIX E: REDUCED PHASE-SPACE DYNAMICS

The fixed-point configurations corresponding to the change of Hamiltonian variables z_i, $z_i^*\rightarrow\xi_a$ ϕ_a, N, ψ are obtained from the equations of motion rewritten in terms of the new variables (see below). Coordinates transformation (23) can exhibit (isolated) singular points where they are not invertible. Dimer configurations with an empty well provides an explicit example where transformations (23) are ill defined. In fact, fixed points

$$(z_i)=(\sqrt{N/2}\exp i\phi,0,\sqrt{N/2}\exp i(\phi+\pi))$$

correspond to the set $\{(0,0,\chi,\pi-\chi)|\forall\ \chi\}$, in the new description. As regards dynamical applications, fortunately, this problem is bypassed because the trajectories chosen near the periodic orbits associated to this kind of fixed points (as well as the PS used to study the dynamics near the same fixed points) do not contain, by construction, such pathological points. Upon setting $\phi_{12}:=\phi_1+\phi_2$, $s:=UNt$, the motion equations in the *reduced* phase space are given by

$$\frac{d\phi_1}{ds}=1-2\xi_1+\xi_2+\frac{\tau}{2}\left[\sqrt{\frac{1+\xi_2}{\xi_1-\xi_2}}\cos\phi_2+\frac{(1-2\xi_1+\xi_2)\cos\phi_1}{\sqrt{(1-\xi_1)(\xi_1-\xi_2)}}-\sqrt{\frac{1+\xi_2}{1-\xi_1}}\cos\phi_{12}\right], \tag{E1}$$

$$-\frac{d\phi_2}{ds}=1-\xi_1+2\xi_2+\frac{\tau}{2}\left[\sqrt{\frac{1-\xi_1}{\xi_1-\xi_2}}\cos\phi_1+\frac{(1-\xi_1+2\xi_2)\cos\phi_2}{\sqrt{(\xi_1-\xi_2)(1+\xi_2)}}-\sqrt{\frac{1-\xi_1}{1+\xi_2}}\cos\phi_{12}\right], \tag{E2}$$

$$\frac{d\xi_1}{ds}=\tau\sqrt{(1-\xi_1)(\xi_1-\xi_2)}\sin\phi_1+\tau\sqrt{(1-\xi_1)(1+\xi_2)}\sin\phi_{12}, \tag{E3}$$

$$\frac{d\xi_2}{ds}=\tau\sqrt{(\xi_1-\xi_2)(1+\xi_2)}\sin\phi_2+\tau\sqrt{(1-\xi_1)(1+\xi_2)}\sin\phi_{12}. \tag{E4}$$

[1] M.H. Anderson *et al.*, Science **269**, 198 (1995); C.C. Bradley *et al.*, Phys. Rev. Lett. **75**, 1687 (1995).
[2] M.R. Andrews *et al.*, Science **275**, 637 (1997); N.R. Thomas, A.C. Wilson, and C.J. Foot, Phys. Rev. A **65**, 063406 (2002).
[3] B.P. Anderson and M.A. Kasevich, Science **282**, 1686 (1998); S. Burger *et al.*, Phys. Rev. Lett. **86**, 4447 (2001); O. Morsch *et al.*, *ibid.* **87**, 140402 (2001); S. Burger *et al.*, Europhys. Lett. **57**, 1 (2002).
[4] P. Pedri *et al.*, Phys. Rev. Lett. **87**, 220401 (2001).
[5] F.S. Cataliotti *et al.*, Science **293**, 843 (2001).
[6] A. Polkovnikov, S. Sachdev, and S.M. Girvin, Phys. Rev. A **66**, 053607 (2002).
[7] V.V. Konotop and M. Salerno, Phys. Rev. A **65**, 021602 (2002); B. Wu, R.B. Diener, and Q. Niu, *ibid.* **65**, 025601 (2002); B. Wu and Q. Niu, *ibid.* **64**, 061603 (2001).
[8] N. Tsukada, Phys. Rev. A **65**, 063608 (2002).
[9] G.J. Milburn *et al.*, Phys. Rev. A **55**, 4318 (1997); M.J. Steel and M.J. Collett, *ibid.* **57**, 2920 (1998).
[10] R. Franzosi, V. Penna, and R. Zecchina, Int. J. Mod. Phys. B **14**, 943 (2000).
[11] K. Nemoto *et al.*, Phys. Rev. A **63**, 013604 (2001).
[12] B. Wu and Q. Niu, Phys. Rev. A **61**, 023402 (2001).
[13] R. Franzosi and V. Penna, Phys. Rev. A **65**, 013601 (2002).
[14] C. Menotti *et al.*, Phys. Rev. A **63**, 023601 (2001); R. Franzosi, V. Penna, *ibid.* **63**, 043609 (2001).
[15] M. Plesch and V. Buzek, Phys. Rev. A **67**, 012322 (2003).
[16] L. Amico and V. Penna, Phys. Rev. Lett. **80**, 2189 (1998); L. Amico and V. Penna, Phys. Rev. B **62**, 1224 (2000).
[17] A.S. Parkins and D.F. Walls, Phys. Rep. **303**, 1 (1998).
[18] D. Hennig *et al.*, Phys. Rev. E **51**, 2870 (1995).
[19] L. Salasnich, Phys. Lett. A **266**, 187 (2000).

[20] M. Cerruti-Sola and M. Pettini, Phys. Rev. E **53**, 179 (1996).
[21] G. Iacomelli and M. Pettini, Phys. Lett. A **212**, 29 (1996); L. Casetti, M. Pettini, and E.G.D. Cohen, Phys. Rep. **337**, 237 (2000).
[22] M. Pettini, Phys. Rev. E **47**, 828 (1993).
[23] S. Flach and V. Fleurov, J. Phys.: Condens. Matter **9**, 7039 (1997).
[24] M. Plesch and V. Buzek, Phys. Rev. A (to be published).
[25] R. Ionicioiu and P. Zanardi, Phys. Rev. A **66**, 050301(R) (2002).
[26] L. Casetti and V. Penna, J. Low Temp. Phys. **126**, 455 (2002).
[27] F. Dalfovo *et al.*, Rev. Mod. Phys. **71**, 463 (1999); W. Courteille *et al.*, Laser Phys. **11**, 659 (2001).
[28] A.J. Leggett, Rev. Mod. Phys. **73**, 307 (2001).
[29] W.M. Zhang *et al.*, Rev. Mod. Phys. **62**, 867 (1990).
[30] Apparently, a further case should be considered, which is described by the conditions $x_1, x_2 \neq x_3$, $x_1 \neq x_2$. This case can be shown to have no solution.
[31] It is important to stress the fact that the coordinate change expressed by definitions (23) is well defined only for $z_1, z_2, z_3 \neq 0$. Therefore, situations where such particular points are involved—fixed points of the π-state case provide an example of this pathology—must be dealt with with some caution.
[32] An alternative method to associate classical chaotic trajectories to quantum systems, based on Bohm's formulation of quantum mechanics, has been proposed in Ref. [21].
[33] E. Ott, *Chaos in Dynamical Systems* (Cambridge University Press, Cambridge, 1993); B. Wu, R.B. Diener, and Q. Niu, Phys. Rev. A **66**, 023404 (2002).